X. DSIF Development

DEVELOPMENT AND IMPLEMENTATION

A. CTA 21 to TRW Passive Microwave Link,

M. E. Wyatt

1. Introduction

To establish compatibility between the DSN and the various spacecraft prior to launch, Compatibility Test Area 21 (CTA 21) was implemented at JPL to represent a standard DSIF station. Via microwave link, CTA 21 can establish compatibility with a spacecraft in the Spacecraft Assembly Facility, the Environmental Test Laboratory, or the Space Simulator. However, the *Pioneer* Project has determined it impractical to bring the *Pioneer F* and *G* spacecraft to JPL for the necessary compatibility tests. Therefore, it has been proposed that an S-band microwave link be established between CTA 21 and TRW in Redondo Beach so that the compatibility tests may be integrated with the presently scheduled tests at TRW.

2. Plan

The plan at present is to establish a test link between JPL and TRW to determine if an operational S-band link is feasible over this path at the available signal levels. If the test link proves feasible, a permanent installation is planned.

When clearance to transmit S-band is received, it is planned to first set up an EMA910 field intensity receiver (borrowed from the JPL Electromagnetic Interference Group) on TRW Building M2 (2 story) with a tripod-mounted antenna to determine the signal and noise levels at the DSIF frequencies and to determine the amplitude modulation of a carrier transmitted from an HP8614 frequency generator with synthesizer and tripod-mounted antenna located at Henninger Flats in Angeles National Forest.

If preliminary tests indicate that the link direct to Building M2 is very unstable, the feasibility link will be set up with another relay on Building E2 (7 story), if TRW consents.

The feasibility link will consist of 4- or 6-ft antennas as follows: a 6-ft antenna at CTA 21 (existing), two back-to-back antennas at Henninger Flats, one antenna on M2 at TRW, and, if required, two antennas back-to-back on Building E2 at TRW. The exciter and receiver at CTA 21 will be used in conjunction with a test transponder to establish the phase and amplitude characteristics of the link. If determined feasible, the final link will consist of 6-ft dishes throughout.

3. Status

The task was assigned on June 23, 1970 and a clearance to transmit 2295 and 2110 MHz was requested along with a "use permit" to establish a relay site in the Angeles National Forest. A temporary use permit (effective until September 1, 1970) to set up a temporary relay site in the Angeles National Forest has been received. On July 30, the RF clearance was received but no testing has been accomplished.

Studies of topographic maps indicated several sites in the San Rafael Hills (south of JPL) and in the Angeles National Forest (east of JPL) could be used as relay points for one-bounce between JPL and TRW. However, the San Rafael Hills are private or city property and investigations have indicated that negotiations with the U. S. Forestry Service would be the most feasible and expeditious because JPL has secured "use permits" from the U. S. Forestry Service before.

Further investigations using helicopter and topographic maps indicate that the Henninger Flats helipad area would provide the optimum location because (1) it can be seen from JPL and TRW, (2) it is accessible by helicopter or car, (3) it extends the largest angle between the JPL mesa and CTA 21, and (4) it extends the largest angle between JPL and TRW.

B. Waveguide Switch Protector, *R. B. Kolbly*

The waveguide switches used by the Deep Space Instrumentation Facility are driven by a gear-reduced dc motor, with no power supplied to the motor armature with the switch in its operating position. If, for any reason, the motor operates with the switch rotor "hung up," the motor will destroy itself. A fuse is provided, but it is required to protect several switches, and does not reliably protect an individual switch motor.

In general, waveguide switch failures can be divided into two types:

(1) The switch rotor "hangs up" between positions, preventing the rotor from reaching its intended position. The motor continues to receive power, eventually burning it up.

(2) An internal relay or limit switch fails, allowing the motor to continue to operate, even though the switch rotor has reached a mechanical stop.

The common feature of these two types of failure is that the motor continues to draw power for an excessive period of time, until it destroys itself. The key to protection then is to sense when the motor is operating for an excessive period of time.

The circuit of this waveguide switch protector consists of a timing pulse generator, a counter, a current detector, and relay and alarm circuits. Figure 1 is a block diagram of the basic protection unit.

In this device, 60-Hz line voltage is converted to timing pulses by means of an *exclusive or* circuit utilizing a μL914 dual two-input gate. These pulses are applied to a $\div 256$ circuit (FF1–FF8). During the period when the waveguide switch is not being operated, the reset line of FF1–FF8 is high (approximately +3.6 V), preventing the flip-flops from counting. When the waveguide switch is activated, a sharp increase in voltage occurs at the output of the current-sensing transformer, which in turn is rectified and inverted by I1, causing the flip-flop reset lines to go low, allowing the counter chain to count the 60-Hz pulses. If the waveguide switch completes its cycles and the motor stops before FF8 is "set" (approximately two seconds), the output of the inverter goes high, forcing all flip-flops to set and stop the count, effectively returning the circuit to its starting point.

If the waveguide switch does not stop drawing current before FF8 is set, there is trouble within the switch. In this case, when FF8 is set, relay K1 is closed, giving an external alarm to the operator and removing power from the waveguide switch by means of slave relay K2. One set of contacts on K1 is used to hold K1 closed until the circuit is manually reset. This prevents the circuit from automatically recycling, which would set up an oscillation, causing eventual destruction of the switch motor.

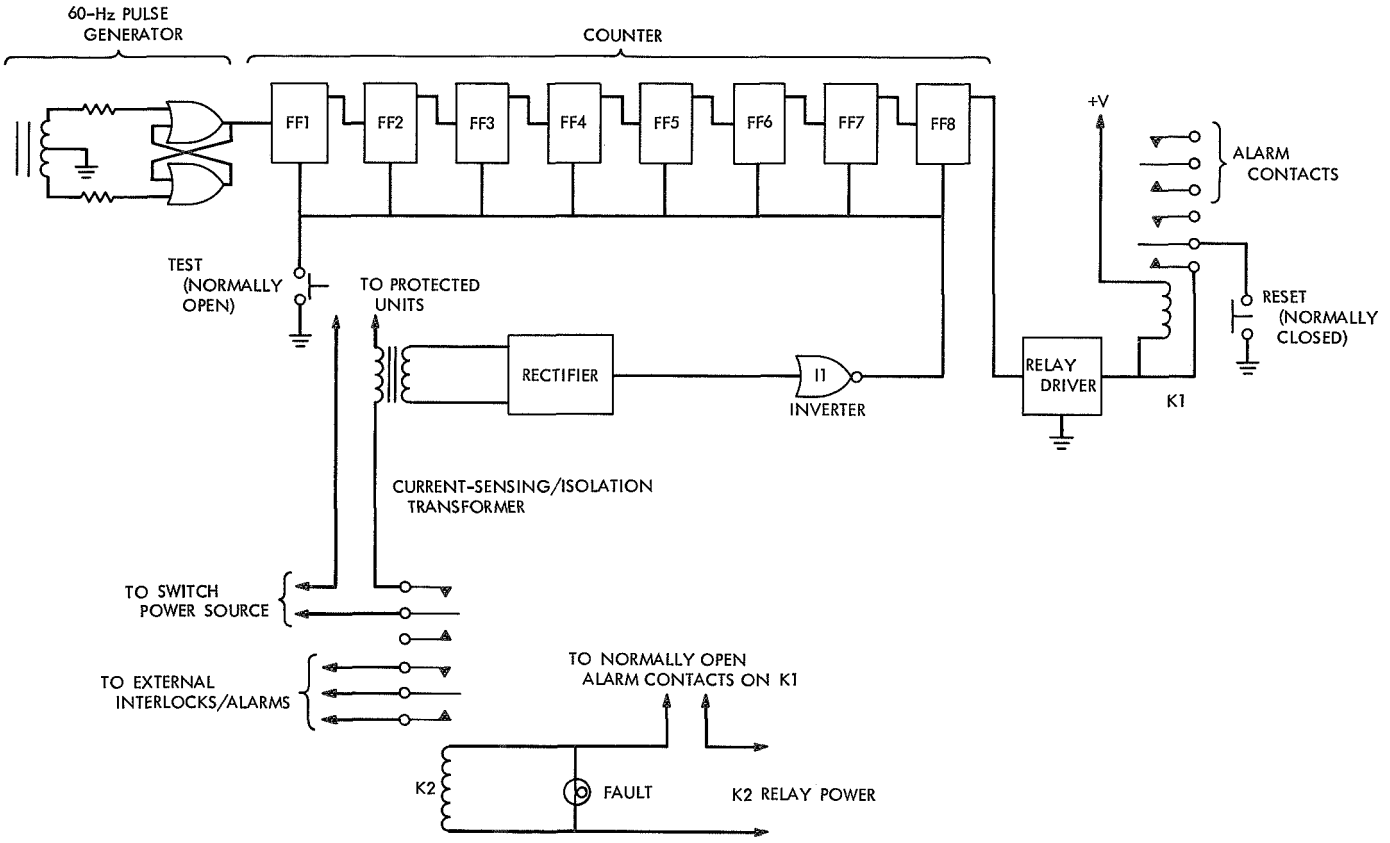

Fig. 1. Waveguide switch protector

A *test* function is provided to enable the operator to determine that the protective circuit is operating properly. A normally open push button is held closed for the two seconds or so required to set FF8 and activate the alarm. Momentary operation of the RESET push button returns the circuit to normal operation.

The time required to activate relay K1 can be changed by modifying the counter chain, or the repetition rate of the pulse generator, or both. By proper selection of the current-sensing transformer and inverter circuit constants, a number of waveguide switches can be protected by this circuit.

In addition to using this circuit to protect waveguide switches, it could be used to protect other types of intermittent-operation devices, such as machine-tool positioners, spacecraft antenna positioners, etc. Because it is digital in operation, this unit is not sensitive to variations in temperature and voltage. Also, it can be made very small and light, as well as low in cost.

C. Block IV Receiver Automatic Carrier Acquisition, R. C. Bunce

1. Introduction

A new method of automatically acquiring down-link (spacecraft) carriers for phase-lock receiver tracking loops has been designed in conjunction with the Block IV DSN Receiver Development Program. The method has been verified as operationally feasible during the prototype receiver checkout at DSS 13. At this station, automatic acquisition of the *Pioneer* and *Mariner* series spacecraft carriers has been achieved, with signal levels in the vicinity of −170 dBmW ±5dB.

As a system function (see Fig. 1), the method combines the frequency sweep capabilities of the programmed local oscillator (PLO) assembly with an automatic acquisition detector. Acquisition search is conducted with the receiver in an open-loop mode, the input to the voltage-controlled oscillator (VCO) being shorted to ground to eliminate false locks. During search the PLO frequency sweeps the receiver local oscillator, tuning across the carrier uncertainty range until zero beat between the carrier and the local receiver reference frequency occurs. At this instant the acquisition detector generates an acquisition-trigger-at-zero-beat (ATZ) signal. The ATZ signal is fed to the PLO, causing it to discontinue sweeping and closes the receiver automatic phase control (APC) loop by removing the VCO ground. The loop then completes acquisition by automatically pulling in to phase lock.

The method and design have been optimized to give a maximum zero-beat signal-to-noise ratio in the acquisition detector channel.

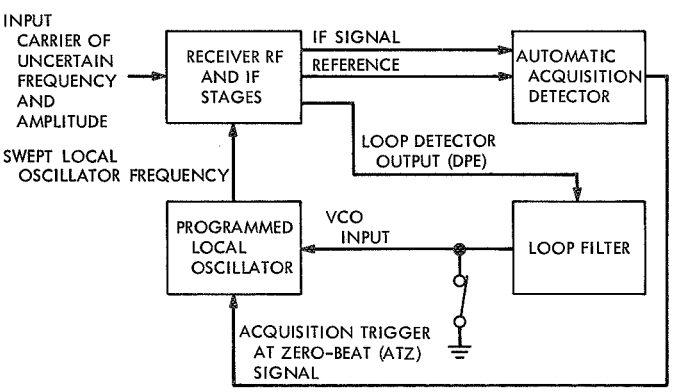

Fig. 1. Block IV automatic acquisition simplified block diagram

2. The Automatic Acquisition Detector

a. General description. The automatic acquisition detector is functionally diagrammed in Fig. 2. The IF signal is fed to the inputs of two identical phase detectors which are referenced in quadrature. The detectors act on the swept signal as frequency-differencing mixers, producing an output of linearly varying frequency that passes through zero beat as the swept signal frequency passes the receiver reference frequency. At zero beat, the multiplier outputs are voltages proportional to the arbitrary phase angle of the signal at that instant, which cannot be predicted. However, since the detectors are in quadrature, the phase difference between these two outputs (e_s and e_c) is 90 deg. (See Table 1 for definitions of symbols used in this article.) This quadrature is necessary to hold the trigger-pulse level constant. Errors in the 90-deg quadrature reference angle lead to amplitude variations in the trigger-pulse height; such errors must be minimized for stable and repeatable operation. Typical signal waveforms e_s and e_c for a linear

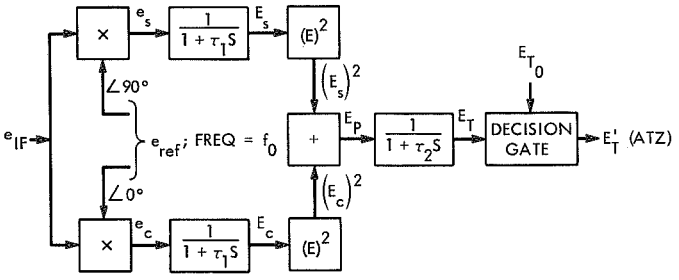

SIGNAL FREQUENCIES (HIGH-ORDER TERMS NEGLECTED):

FREQ $(e_{IF}) = 2\pi f_0 + 2\pi \dot{f}\tau$ (rad/sec); $-T \le \tau \le t$, $t = 0$ AT ZERO BEAT

FREQ $(e_{ref}) = 2\pi f_0$ (rad/sec)

FREQ $(e_s, e_c) = 2\pi \dot{f}\tau = \dot{\phi} = d\phi/d\tau$, $\dot{f}$ = SWEEP RATE, Hz/sec

PHASE (LINEAR SWEEP):

$$\text{PHASE } (e_s) = \int_{-T}^{t} \dot{\phi}(\tau)\, d\tau = \pi \dot{f} t^2 + \phi_0, \quad \left[\phi_0 = -\pi \dot{f} T^2 + \phi(-T)\right]$$

$$\text{PHASE } (e_c) = \int_{-T}^{t} \dot{\phi}(\tau)\, d\tau + \frac{\pi}{2} = \pi \dot{f} t^2 + \phi_0 + \frac{\pi}{2}$$

WAVEFORMS:

$$e_s = A \sin\left(\pi \dot{f} t^2 + \phi_0\right) \qquad e_c = A \cos\left(\pi \dot{f} t^2 + \phi_0\right)$$

$$E_{s,c} = \frac{1}{\tau_1} \int_{-T}^{t} \exp\left[\frac{-(t-\tau)}{\tau_1}\right] e_{s,c}(\tau)\, d\tau \qquad E_P = E_s^2 + E_c^2 \text{ [INDEPENDENT OF } \phi_0]$$

$$E_T = \frac{1}{\tau_2} \int_{-T}^{t} \exp\left[\frac{-(t-\tau)}{\tau_2}\right] E_P(\tau)\, d\tau \qquad E'_T = \begin{cases} 0, & E_T < E_{T_0} \\ 1, & E_T > E_{T_0} \end{cases}$$

Fig. 2. Automatic acquisition detector functional diagram

Table 1. Nomenclature

A	sine-wave signal peak voltage, V
A_M	signal level at minimum operating condition, V
A_0	design-point signal peak voltage (minimum), V
e_c	multiplier (0 deg or cosine ϕ) output, V
e_{IF}	IF signal (out of limiter), V rms
e_{ref}	multiplier reference signal, V rms
e_s	multiplier (90 deg or sine ϕ) output, V
E_s, E_c	parallel band-pass filter outputs (sine and cosine channels), V
E_P	summing-junction voltage, V (E_{P_S} = signal component when noise is considered; E_{P_N} = noise component)
E_T	post-filter output trigger pulse, V (E_{T_S} = signal component; E_{T_N} = noise component)
E_{T_0}	trigger level for acquisition decision, V
E'_T	decision gate output (binary state), V
f_0	multiplier reference (zero beat) frequency, Hz
$\dot{f}$	sweep rate of signal (around f_0), Hz/sec
$\dot{f}_0$	design value (usually minimum) of $\dot{f}$, Hz/sec
f, f'	frequency, Hz
ΔF_N	frequency error due to noise of trigger point, Hz
K	probability of acquisition, sigma units (normal curve of error integral)
N_0	noise spectral density (referred to receiver output), W/Hz
P	probability density function
P_A	probability of acquisition (zero to unity) per zero-beat pass
P_{TT}	probability of transient (false) triggering; fraction of time noise voltage dwells above E_{T_0}
R	ratio of τ_2/τ_1
t	time, sec
T	time of sweep preceding zero beat, sec
T_{TT}	time between transient triggering
X	independent variable, as defined in text
σ_N^2	variance of noise at summing junction (voltage due to noise power), V
$\sigma_{N_T}^2$	variance of noise at post-filter output, V
τ	normalized time t/τ_1 (dummy variable for t), sec/sec
τ_1	parallel filters time constant, sec
τ_2	post-filter time constant, sec
ϕ	phase angle, rad or deg (ϕ_0 = phase angle at zero beat)

frequency sweep are shown at the top of Fig. 3 for an arbitrary phase difference (ϕ_0) of 60 deg. Note the frequency variation around zero beat and the symmetry with respect to this point.

The effect of a filter on the waveforms e_s and e_c is not easily modeled mathematically; only a rather cumbersome series solution can be obtained in the general case. The function resembles the Fresnel integral, and its value at zero beat can be analytically determined, as shown later. The waveforms shown were machine-integrated, using an approximation to the convolution integral form, and the results were automatically plotted. The integral is noted in Fig. 2 and typical results (E_s and E_c) are shown on Fig. 3. Recorded waveforms during sweep are shown at the top of Fig. 4 for comparison.

When these waveforms are of the same amplitude and are squared and summed, theoretical independence of ϕ_0 is easily established. Upon squaring and summing, not only is the ϕ_0 effect eliminated but, as zero beat is approached, the voltage at the summing junction increases smoothly. This was first observed on a machine plot and later verified on the feasibility model (E_P, Figs. 3 and 4). The smoothness of E_P in the negative regions of t increases as the integrator gain decreases. The approach is far from monotonic when the integrator gain is infinite. Analytical determination of the effect of the integrator is seemingly impossible, since it involves approaching a finite time with negative and positive values from an infinite negative limit; even the series solution was not of much help. However, as a practical result, the method of pre-filtering, squaring, and summing of the signals produces a clean pulse with a smooth rise and rapid decay; the pulse amplitude at zero beat is some fraction of its peak height, and small variations in amplitude follow the peak.

Noise present on E_s and E_c is also detected as part of E_P, where it appears as an average dc value with residual noise variations around it. The zero beat signal level-to-dc noise component ratio was investigated (for fixed sweep rate $\dot{f}$) as a function of the filter time constant τ_1, and found to be optimum for an approximate value of $\tau_1 = [2\pi\dot{f}]^{-1/2}$. The noise variance is theoretically the same as the mean dc noise value. To reduce the probability of noise voltage peaks exceeding the trigger level of the decision gate, a post filter (with time constant τ_2) was added. This filter also has the effect of

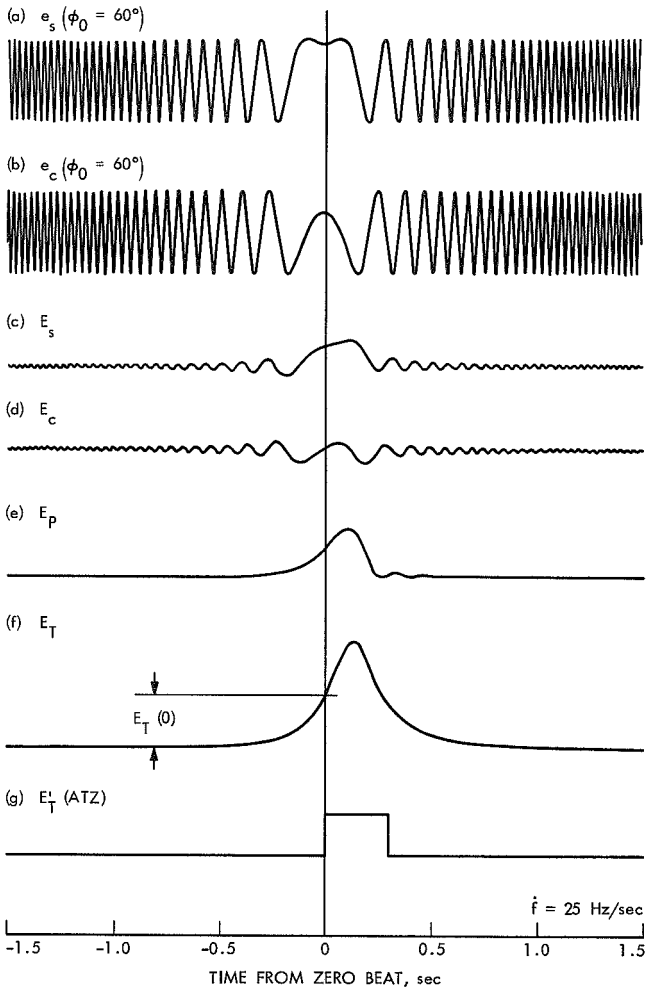

Fig. 3. Theoretical waveforms of acquisition detector

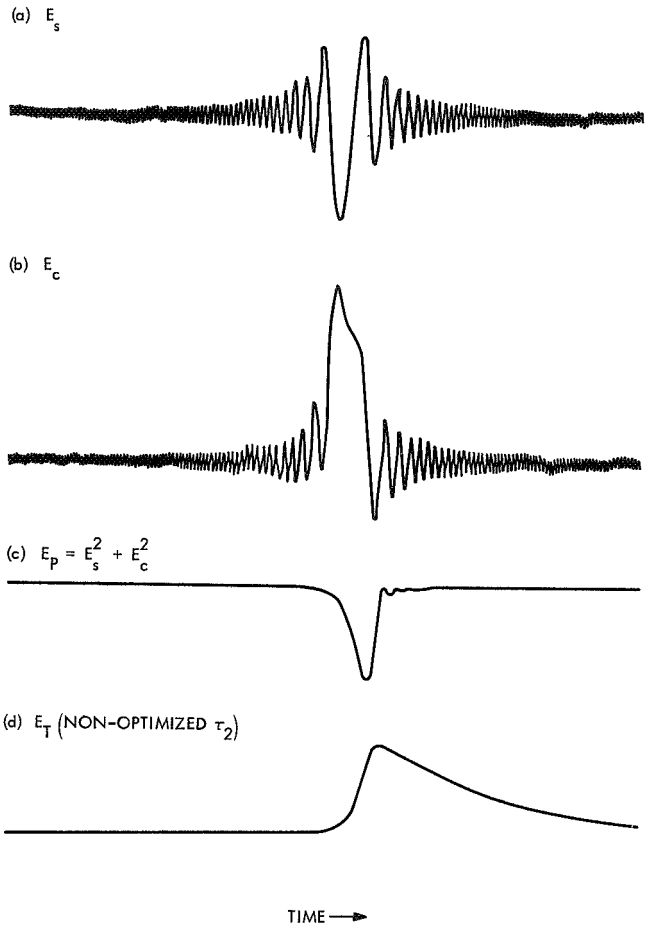

Fig. 4. Actual waveforms of acquisition detector

suppressing the amplitude of the E_P pulse, and its peak value-to-noise variance ratio was also investigated and found to optimize for a value of $\tau_2 \cong 1.68\ \tau_1$. The optimized form of E_T, the signal output of the post filter, is shown in Fig. 3 (machine plot).

The trigger level E_{T_0} is adjusted as a system procedure to equal the zero-beat amplitude of the E_T pulse at a minimum operating signal level (MOC), using a minimum sweep rate for this condition (covered later). At higher signal levels, the sweep rate is increased to suppress the zero-crossing level. In all cases, when the trigger level is exceeded, the decision gate changes state, producing a binary ATZ signal. When the detector is used as part of the acquisition system, the ATZ signal disables the local sweep and closes the receiver APC loop by removing the ground at the VCO input. The receiver then automatically phase locks to the incoming signal. During lock, the ATZ signal is normally a constant dc level, since a constant zero-beat signal is present. However, when the in-lock carrier is noisy, the detected pulse occasionally drops below the trigger level, causing momentary loss of the ATZ signal. A two-second delay is used within the PLO to prevent this type of ATZ loss from falsely initiating a search during in-lock operation; this is covered more fully later.

b. Analysis. The basic mathematical model for the detector channel is given in Fig. 2. A linear frequency sweep and sine-wave signal are assumed in this analysis; higher-order sweep rate terms and carrier frequency jitter that may be present in practice are neglected. The integrals, in general, have no analytic solution and machine integration was used to obtain numerical results and automatically plot the waveforms which led to the optimization of the detector. Most waveforms were functionally verified by comparing with those obtained from operating equipment. The notations on Fig. 2 refer to signal only; when noise is considered in the following expressions, suitable subscripts are used.

The optimizing design criteria and parameter limits are given in expressions (8), (14), (16), (17), and on Figure 11. A list of nomenclature terms is given in Table 1. All gain factors in the following expressions have been normalized to unity.

(1) *Optimization of* τ_1. The summing junction signal voltage is

$$E_{P_S}(t) = \left[\frac{A}{\tau_1}\int_{-T}^{t} e^{-(t-\tau)/\tau_1}\sin(\pi\dot{f}\tau^2+\phi_0)\,d\tau\right]^2 + \left[\frac{A}{\tau_1}\int_{-T}^{t} e^{-(t-\tau)/\tau_1}\cos(\pi\dot{f}\tau^2+\phi_0)\,d\tau\right]^2 \quad (1)$$

and the summing junction noise voltage is

$$E_{P_N}(t) = 2N_0\int_0^\infty \frac{1}{1+(2\pi f\tau_1)^2}\,df + V_n(t,N_0)$$
$$= 2N_0\left|\frac{1}{2\pi\tau_1}\tan^{-1}(2\pi f\tau_1)\right|_0^\infty + V_n(t,N_0)$$
$$= \frac{N_0}{2\tau_1} + V_n(t,N_0) \quad (2)$$

The noise voltage consists of a dc component and time-variable part (N_0 assumed white and gaussian). For large T, at zero beat, expression (1) has the particular solution:

$$\left.\begin{aligned}\lim_{T\to\infty} E_{P_S}(0) &= \pi A^2\left[\frac{1}{2\tau_1\sqrt{\pi\dot{f}}}\right]^2\left[1-2(S_a+C_a)+2(S_a^2+C_a^2)\right]\\ S_a &= \sqrt{\frac{2}{\pi}}\int_0^{1/2\tau_1\sqrt{\pi\dot{f}}}\sin(t^2)\,dt \qquad C_a = \sqrt{\frac{2}{\pi}}\int_0^{1/2\tau_1\sqrt{\pi\dot{f}}}\cos(t^2)\,dt\end{aligned}\right\} \quad (3)$$

The summing junction zero-beat signal-to-noise dc component is

$$|S/N|_{dc\Sigma} = \frac{\lim_{T\to\infty} E_{P_S}(0)}{\frac{N_0}{2\tau_1}} \quad (4)$$

For fixed $\dot{f}$, this varies with τ_1 according to

$$\left.\begin{aligned}|S/N|_{dc\Sigma} &= \frac{A^2}{N_0}\sqrt{\frac{\pi}{\dot{f}}}(X)\left[1-2(S_a+C_a)+2(S_a^2+C_a^2)\right]\\ X &= \frac{1}{2\tau_1\sqrt{\pi\dot{f}}}\\ S_a &= \sqrt{\frac{2}{\pi}}\int_0^X \sin(t^2)\,dt \qquad C_a = \sqrt{\frac{2}{\pi}}\int_0^X \cos(t^2)\,dt\end{aligned}\right\} \quad (5)$$

By numerical integration, expression (5) was found to have a maximum value at

$$X(|S/N|_{dc\Sigma}\,\max) \approx \frac{1}{\sqrt{2}} \text{ (see Fig. 5)} \quad (6)$$

yielding optimum conditions at summing junction:

$$|S/N|_{dc\Sigma}\,\max = \left(\frac{A^2}{N_0}\right)\left(\sqrt{\frac{\pi}{\dot{f}_0}}\right)(0.238)$$
$$= 0.422\frac{A^2}{N_0\sqrt{\dot{f}_0}} \quad (7)$$

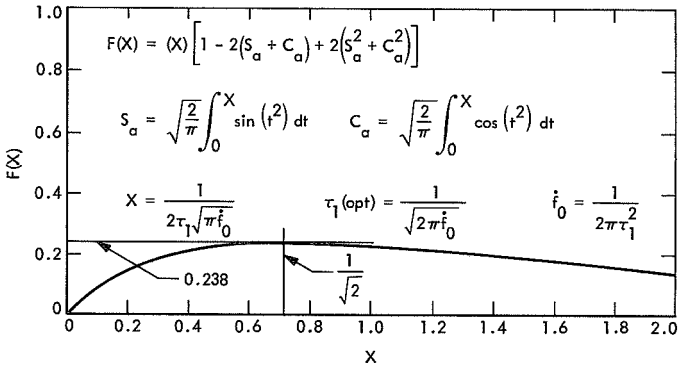

Fig. 5. Optimization of τ_1 for constant $\dot{f}$

and

$$\tau_1\,(\text{optimum}) = \frac{1}{\sqrt{2\pi\dot{f}_0}} \tag{8}$$

where $\dot{f}_0$ is the selected sweep rate for which τ_1 is optimized. The detected pulse shape associated with this optimization is shown on Fig. 6.

(2) Optimization of τ_2. The time-variable component of noise at the summing junction has a spectral density obtained by convoluting the filter output spectral density with itself:

$$S_{V_N}(f) = 4N_0 \int_0^{+\infty} \frac{1}{1+[2\pi\tau_1 f']^2} \times \frac{1}{1+[2\pi\tau_1(f-f')]^2}\,df'$$

$$= \frac{N_0}{2\tau_1} \times \frac{1}{1+(\pi\tau_1 f)^2} \tag{9}$$

The variance of the variable noise component at the post-filter output is therefore:

$$\sigma^2_{N_T} = \frac{N_0}{2\tau_1}\int_0^{\infty} \frac{1}{1+(\pi\tau_1 f)^2} \times \frac{1}{1+(2\pi\tau_2 f)^2}\,df$$

$$= \frac{N_0}{(2\tau_1)^2}\left[\frac{1}{1+\dfrac{2\tau_2}{\tau_1}}\right] \tag{10}$$

The signal at the post-filter output, as the filter time constant varies, can be expressed as (at $\dot{f} = \dot{f}_0$):

$$\left.\begin{aligned} E_{T_S}(\tau) &= \frac{A^2}{R}\int_{-\infty}^{\tau} e^{-(\tau-T)/R}\,E_P(T)\,dT \\ \tau &= t/\tau_1 = \sqrt{2\pi f_0}\,t \qquad R = \tau_2/\tau_1 \\ E_P(T) &= \left[\int_{-\infty}^{T} e^{-(T-\tau)} \sin\left(\frac{\tau^2}{2}\right)d\tau\right]^2 + \left[\int_{-\infty}^{T} e^{-(T-\tau)} \cos\left(\frac{\tau^2}{2}\right)d\tau\right]^2 \end{aligned}\right\} \tag{11}$$

The expression (11) was numerically approximated by machine for various ratios τ_2/τ_1; typical results are shown on Fig. 7. The peak results were divided by expression (10) to yield:

$$\left|S/N\left(\frac{\tau_2}{\tau_1}\right)\right| E_T(\text{PK}) = \frac{[E_{T_S}(\text{PK})]^2}{N_0} \times (2\tau_1)^2 \times \left[1+\frac{2\tau_2}{\tau_1}\right] \tag{12}$$

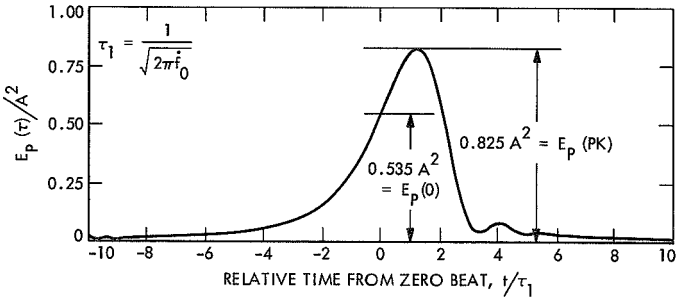

Fig. 6. Optimum detected pulse E_{P_S}

The results, in dB enhancement by the post filter, are shown on Fig. 8. This gave the optimum ratio:

$$R_{\text{opt}} = \frac{\tau_2}{\tau_1}\,(\text{opt}) \approx 1.68 \tag{13}$$

or

$$\tau_2\,(\text{optimum}) \approx 1.68\,\tau_1 \tag{14}$$

The pulse shape is plotted on Fig. 9.

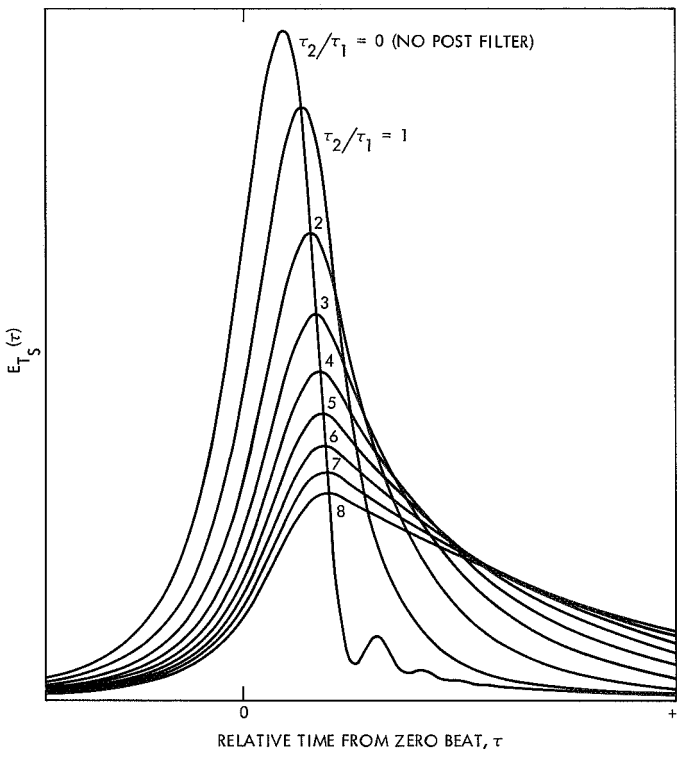

Fig. 7. Effect of post-filter τ_2 on trigger pulse shape

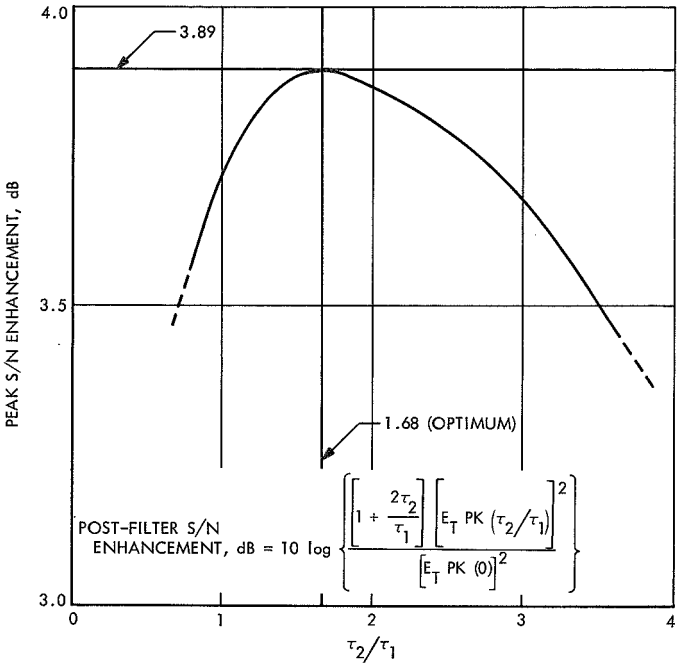

Fig. 8. S/N enhancement as a function of τ_2/τ_1

3. Choice of Minimum Sweep Rate and Trigger level

Assuming the acquisition system is associated with a receiver reference loop of design-point bandwidth $2B_{L_0}$, then the mean-peak-trigger-pulse-signal-voltage-to-noise-dc-voltage ratio at the receiver loop design point will be (from expression 2 and Fig. 9), gain normalized:

$$E_{T_N}(\text{dc}) = \text{noise dc} = \frac{N_0}{2\tau_1}$$

$$\text{signal (design pt)} = N_0(2B_{L_0}) = \frac{A_0^2}{2}$$

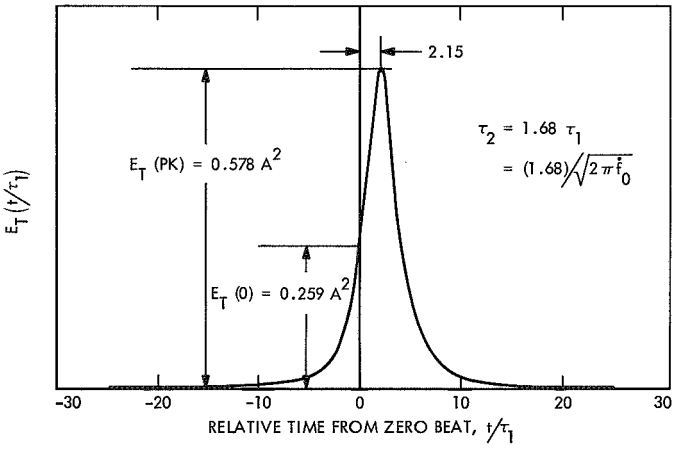

Fig. 9. Optimum trigger pulse E_{T_S}

$$\frac{\text{mean peak signal}}{\text{noise dc}} = \frac{0.578\,A^2}{\frac{N_0}{2\tau_1}} = \frac{1.156\,N_0(2B_{L_0})}{N_0} \times (2\tau_1)$$

$$= 1.156(2B_{L_0}) \times \frac{2}{\sqrt{2\pi \dot{f}_0}} = 0.922\left[\frac{2B_{L_0}}{\sqrt{\dot{f}_0}}\right] \qquad (15)$$

Choosing this ratio as *unity* (compatible with main loop design point criteria) yields

$$\dot{f}_0 \approx 0.850\,(2B_{L_0})^2 \text{ Hz/sec} \tag{16}$$

The optimum setting for the trigger level is a function of the signal level and sweep rate; it is obvious that the least acquisition error will occur if the trigger-pulse amplitude (nominal) crosses the trigger level at zero beat. If the sweep rate of expression (16) is used at an arbitrary low signal level, the correct setting is

$$\frac{E_{T_0}}{E_{T_N}} = 1 + 0.448\left(\frac{A_M}{A_0}\right)^2 \tag{17}$$

where E_{T_N} is the dc noise component at the post-filter output in the absence of signal, and A_M is an arbitrary minimum-operating-condition (MOC) signal level discussed more fully later. At the MOC, acquisition trigger-point frequency error is a function of the signal level uncertainty and the amplitude displacement due to noise. At signal levels above the MOC, the sweep rate is increased to suppress the zero-crossing level. Machine integration yielded the suppression shown on Fig. 10, which is expressed in dB on Fig. 11. In the Block IV equipment, the MOC is set at $A_M = \sqrt{10}\ A_0$ (10-dB margin). Above this level the sweep rate is increased to compensate for the signal level increase corresponding to the suppression factor given on Fig. 11. Limiter action restricts the maximum sweep rate to about:

$$\dot{f} \text{ max (strong signal)} \approx 20\,\dot{f}_0 \tag{18}$$

corresponding to a total signal level range of 23 dB at the limited output.

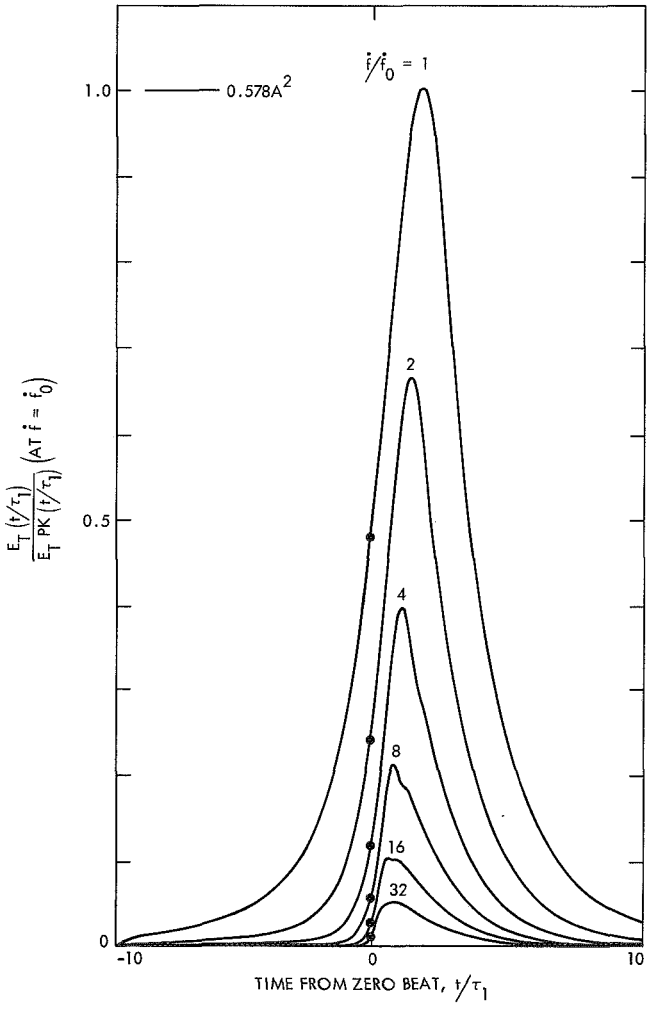

Fig. 10. Trigger pulse suppression as a function of sweep rate

4. Acquisition Probabilities and Trigger Error

The probability of acquisition is directly related to the probability of the pulse (Fig. 9) exceeding the trigger level E_{T_0} as the signal passes through zero beat. This does not imply that this event will occur at $t = 0$; the acquisition decision will, in general, occur with a frequency error associated with the precise time at which the pulse amplitude, perturbed by noise and

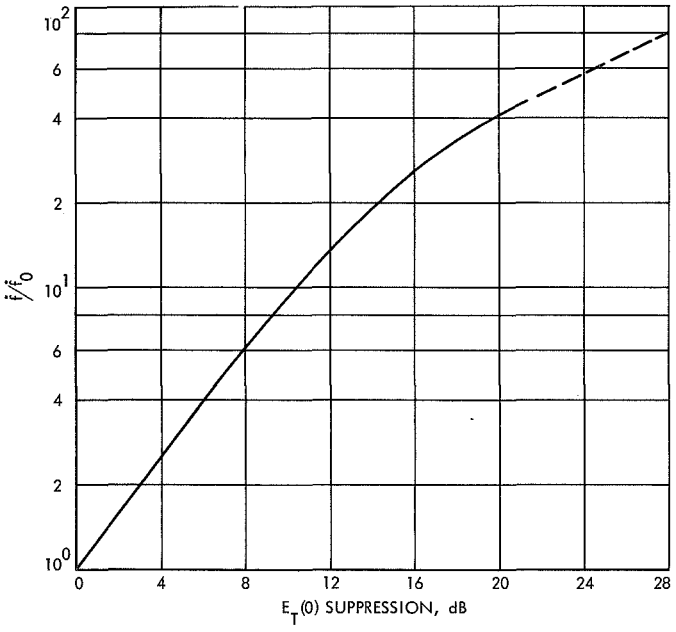

Fig. 11. Zero-crossing amplitude suppression as a function of sweep rate

signal level uncertainty, crosses the trigger level. However, as long as this error does not exceed the acquisition bandwidth of the main receiver loop, acquisition will occur.

A full statistical study of the subject amplitude has not been attempted; however, a lower bound on this probability can be estimated for the signal level region in which the trigger level is set based on the minimum expected signal level:

$$\text{Probability of acquisition (min)} = P_A = \frac{1}{2} + \text{erf}\,[K_1]$$

$$K_1 \approx \left[1 - \sqrt{\frac{0.259}{0.578}}\right]\frac{A}{A_0} \tag{19}$$

This probability is the major bound on the arbitrary MOC selection. At $A = A_0$, this is about 0.71/pass; at $A = \sqrt{10}\ A_0$, the selected Block IV MOC, this is about 0.96/pass. These figures assume that the pulse amplitude variance is gaussian and equal to that of the noise at $A = A_0$. The actual probability undoubtedly exceeds this, since the pulse variance occurs in the entire region of zero beat, not simply at the instant of peak amplitude, as expression (19) implies. Under stronger signal conditions, even if sweep rate is increased to suppress the pulse amplitude, P_A will continue to increase as the signal suppression factor increases, decreasing the relative signal variance.

The probability of a transient ATZ signal occuring is the same as the probalility of a noise spike exceeding the trigger level and will cause a short false decision period in the absence of signal. The moments of the probability density function (PDF) at the post-filter output are very cumbersome to calculate, and this was not attempted. The PDF at the summing junction, however, can be shown to be exponential (variable noise component only):

$$\left.\begin{aligned} P(E_{P_N}) &= \frac{1}{(\sigma_N)^2}\exp\left[-\frac{E_{P_N}}{(\sigma_N)^2}\right] \\ \sigma_N^2 &= \frac{N_0}{(2\tau_1)^2} \end{aligned}\right\} \tag{20}$$

This was roughly confirmed by sample data taken on the feasibility model. The optimized ratio of expression (12) results in a variance reduction of

$$(\sigma_{N_T})^2 = \left[1 + \frac{2\tau_2}{\tau_1}\right]^{-1}(\sigma_N)^2 = 0.229\,(\sigma_N)^2 \tag{21}$$

The PDF of this function tends away from the exponential toward the Rayleigh (Ref. 1); however, solutions available in the literature are only approximate, and most treat only the signal-plus-noise case. A rough approximation can be obtained, however, by simply substituting σ_{N_T} of expression (21) into expression (20) and integrating to obtain the approximate cumulative function:

$$P(E_{T_N} > E_{T_0}) \approx 1 - \int_0^{E_{T_0}} \frac{1}{0.229(\sigma_N)^2}\exp\left[-\frac{X}{0.229(\sigma_N)^2}\right]dX$$

$$\approx \exp\left[-\frac{E_{T_0}}{0.229(\sigma_N)^2}\right] \approx P_{TT} \tag{22}$$

The probability of transient (false) triggering, P_{TT}, must be interpreted carefully; it simply represents an estimate of the fraction of time that the noise voltage exceeds E_{T_0}, and is not in itself a "mean time between transients." This can be estimated by imagining a sample rate at twice the post-filter bandwidth; that is,

$$\overline{T_{TT}} \approx 4\exp\left[\frac{E_{T_0}}{0.229(\sigma_N)^2}\right]\tau_2, \qquad (\sigma_N)^2 = E_{T_N}$$

or, using expressions (17), (16), (8), and (14),

$$\overline{T_{TT}} \approx \frac{2.91}{(2B_{L_0})}\exp\left[4.37 + 1.96\left(\frac{A}{A_0}\right)\right]^2 \text{ seconds}$$

$$= \text{estimated mean time between transient triggering} \tag{23}$$

At design point ($A = A_0$), expression (23) is

$$\overline{T_{TT}}\,(\text{min}) \approx \frac{1633}{2B_{L_0}} \text{ seconds} \tag{24}$$

In the Block IV system, this is a minimum of 16 seconds for the $2B_{L_0}$ max (design value) of 100 Hz. Expression (23) clearly becomes large enough to be disregarded at $(A/A_0)^2 = 10$, the "MOC." At this point,

$$\overline{T_{TT}} \approx \left[\frac{7.5 \times 10^{10}}{2B_{L_0}}\right] \text{ seconds} \tag{25}$$

Table 2. Block IV R&D receiver automatic acquisition design parameters

Predetection Bandwidth B_G, Hz	Closed-loop Bandwidth $2B_{L_0}$, Hz	Minimum sweep rate $\dot{f}_0$ at MOC, Hz/sec	Maximum sweep rate $\dot{f}$ at strong signal, Hz/sec	τ_1, sec	τ_2, sec
200	1.0 (3.0)	0.85	16.9	0.433	0.727
2000	10.0 (30.0)	85	1690	0.0433	0.0727
20000	100.0 (300.0)	8500	169000	0.00433	0.00727

Frequency errors at the trigger instant occur from two sources: (1) displacement of $E_T(0)$ by noise perturbations, and (2) by errors in the estimate of the signal amplitude A (see Fig. 9). The order of magnitude of the first is that resulting from the peak displacement in time; that is, at the MOC:

$$\Delta F_N\,(\text{order of magnitude}) = 0.923\,(2B_{L_0}) \qquad (26)$$

This is at least an order of magnitude less than the acquisition bandwidth of loops in the receiver under design; additional displacements due to errors in signal amplitude estimates would thus have to be very large to prevent acquisition after triggering. Statistical measurements on the feasibility model showed that the error stated above is apparently normally distributed, and that expression (26) represents about 2 standard deviations of the error distribution.

5. Design Values and Performance of the Block IV R&D Receiver

The Block IV R&D receiver has six closed-loop design point bandwidths with three associated predetection filters, one for each two closed-loop bandwidths. To simplify the design of the automatic acquisition detector, three sets of time constants and associated gain changes were used, one set for each predetection filter. The receiver bandwidths used for the design are the narrower of the two possible in each case to assure acquisition in both modes. Final figures are summarized in Table 2. All spacecraft carrier acquisition to date has been done in the 3-Hz mode, using the figures in the first row of the table. All conditions shown on the table are, however, selectable in the hardware.

Actual recommended sweep rates at the PLO (1/24 of S-band rate) in use at DSS 13 in the narrow-band mode and for the stated MOC, using a value of system temperature of 20°K, are given in Table 3 as a function of carrier level. The rates were derived generally from Fig. 11 and are added to the signal doppler rate to achieve minimum trigger frequency error. The signal level range covers the expected signal levels of the *Mariner* and *Pioneer* spacecraft.

Table 3. Acquisition sweep rate as a function of expected signal level (Block IV receiver, DSS 13)

Signal level, dBmW	Sweep rate at PLO, Hz/sec	Sweep rate at S-band, Hz/sec
−175	0.04	0.85
−174	0.04	0.9772
−173	0.05	1.2410
−172	0.07	1.6358
−171	0.09	2.1544
−170	0.12	2.7877
−169	0.15	3.5243
−168	0.18	4.3508
−167	0.22	5.2510
−166	0.26	6.2068
−165	0.30	7.1979

The Block IV receiver system does not achieve the low probability of expression (25) for an MOC of 10 dB above the 1-Hz design point. An occasional false ATZ signal occurs for reasons not fully understood. The period implied by expression (25) was, however, achieved on the feasibility model evaluated in the laboratory. The causes of the periodic false triggering in the Block IV receiver are presently under investigation. The problem is not serious since a transient triggering, not followed by receiver lock, merely causes a two-second delay in acquisition.

An additional problem arose while acquiring the *Pioneer IX* spacecraft. During this acquisition, ATZ instability led to the need for a manual over-ride procedure to maintain phase lock after acquisition. The instability was not unexpected; the spacecraft signal level was near the MOC and probably had a somewhat broad spectrum. However, to assure stable operation under such conditions, the modification that added a two-second delay within the PLO was implemented. This modification delays the initiation of PLO sweep and loop-opening for two seconds after loss of the ATZ signal. If the ATZ signal reoccurs during the two-second interval, lock is not interrupted. The interval represents the approximate maximum pull-in time for a 1-Hz loop when the frequency error is within the pass-band of the acquisition detector. The delay is, in effect, additional filtering required in the vicinity of zero beat to assure stable acquisition for weak signals. The modification also causes a momentary delay during search in the event that a noise pulse exceeds the ATZ trigger level. The only effect in this case is a longer acquisition period, which is probably increased by not more than 10%.

In summary, the Block IV open-loop acquisition method appears to be a distinct improvement over the Block III design since it avoids inherent false-lock conditions and gives promise of performing automatically over the entire signal level dynamic range. It is not theoretically as rapid as a fully computerized process (such as automatic spectral analysis by fast-fourier transform) might prove to be; however, it is considerably less complex and expensive than the computer approach.

Reference

1. Davenport, W. B., and Root, W. L., *Random Signals and Noise*, p. 199. McGraw-Hill Book Co., Inc., New York, 1958.

D. The Recording of SDA Outputs for *Mariner* Mars 1971, *G. Hamilton*

In the event of failure in the data path after the subcarrier demodulator assembly (SDA), in such a manner that the telemetry and command processor (TCP) tapes do not furnish all required data, it is desirable that the output of the SDA be recorded for possible playback at a later time and insertion into the symbol synchronizer assembly (SSA) for recovery of data at the station. It is a requirement of *Mariner* Mars 1971 that, for this purpose, data be recorded prior to integration. It is also necessary to make provisions for recording two channels (engineering and science) simultaneously for each of two spacecraft. In addition, science may use either a low or high data rate channel. Because of other requirements on the recording subsystem, only two channels are available for recording SDA outputs.

Signal characteristics for recording purposes are as follows:

SDA	Data	Characteristics[a]
A	Engineering	33 bits/s, rectangular waveform, 5-V signal + noise
B	Science	50 bits/s to 10.8 kilosymbols, rectangular waveform, 5-V signal + noise
C	Engineering	33 bits/s, rectangular waveform, 5-V signal + noise
D	Science	50 bits/s to 10.8 kilosymbols, rectangular waveform, 5-V signal + noise

[a]At DSS 14, science data rate is 50 bits/s to 86 kilosymbols.

Since the required dynamic range is so large, i.e., noise plus signal is large compared to the signal, a recording technique which provides good accuracy (1%) and is reasonably conservative of bandwidth and which extends to zero frequency is indicated. The technique which best satisfied these criteria is wideband FM (±40% deviation) multiplexing on a direct record track.

Configuration of the multiplex equipment for the *Mariner* Mars 1971 85-ft stations will be SDAs A and B, representing spacecraft 1, multiplexed together using voltage-controlled oscillators (VCOs) with 13.5- and 108-kHz center frequencies, respectively (Fig. 1). The mixed data will be fed to a mixer amplifier and recorded on tape using direct recording techniques. The bandwidth required is 183.6 kHz (108 kHz × 1.40 + 3 × 10.8). This indicates a recording speed of 15 in./s during encounter. SDAs C and D are processed identically.

At the 210-ft site (DSS 14), VCOs with 13.5 and 525-kHz center frequencies will be used. The bandwidth required is 994.2 kHz (525 kHz × 1.40 + 3 × 86.4). This dictates a recording speed during encounter of 120 in./s.

Suitable discriminators are also being furnished for verification of recordings and VCO setup and for possible playback of a selected recorded SDA output into the SSA, if required.

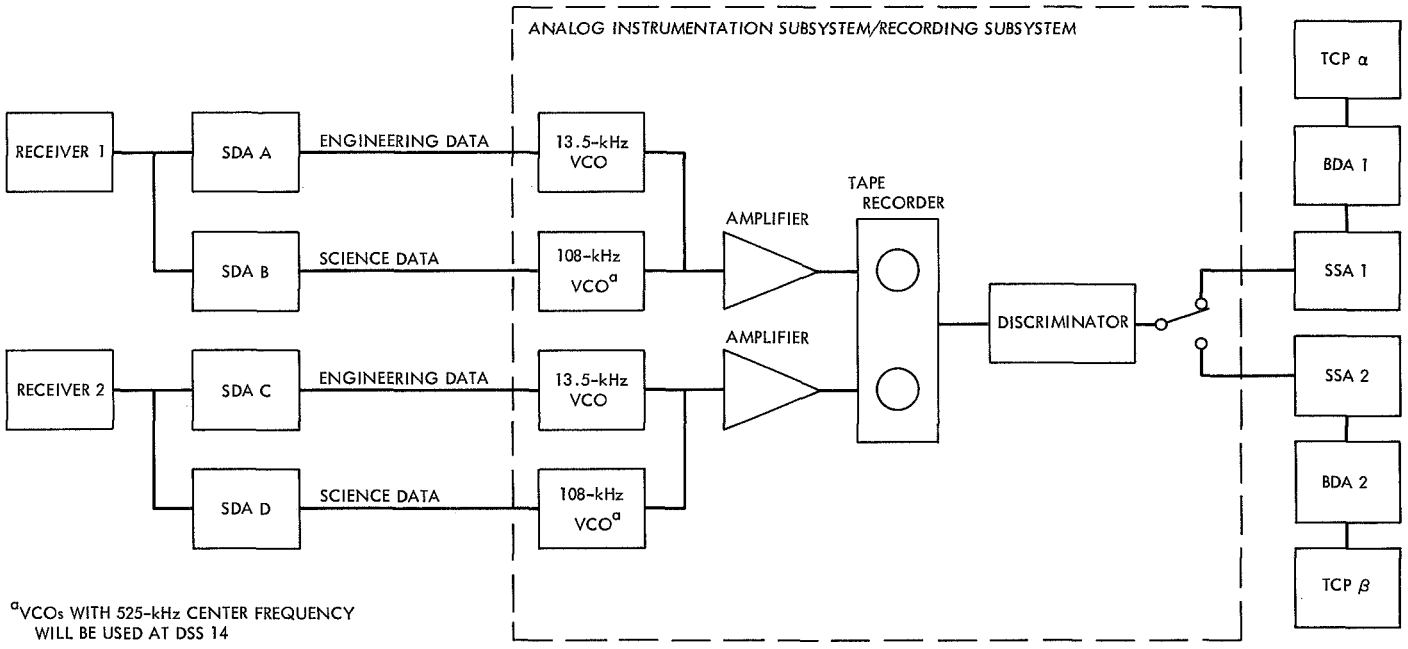

Fig. 1. *Mariner* Mars 1971 SDA output recording and playback data path